Huge Direct Numerical Simulation of Turbulent Combustion -Toward Perfect Simulation of IC Engine-

Mamoru Tanahashi*

* Department of Mechanical and Aerospace Engineering, Tokyo Institute of Technology, Tokyo, Japan
(Tel : +81-3-5734-3181; E-mail: mtanahas@mes.titech.ac.jp)

Abstract: Current state and perspective of DNS of turbulence and turbulent combustion are discussed with feature trend of the fastest supercomputer in the world. Based on the perspective of DNS of turbulent combustion, possibility of perfect simulations of IC engine is shown. In 2020, the perfect simulation will be realized with 30 billion grid points by 1EXAFlops supercomputer, which requires 4 months CPU time. The CPU time will be reduced to about 4 days if several developments were achieved in the current fundamental researches. To shorten CPU time required for DNS of turbulent combustion, two numerical methods are introduced to full-explicit full-compressible DNS code. One is compact finite difference filter to reduce spatial resolution requirements and numerical oscillations in small scales, and another is well-known point-implicit scheme to avoid quite small time integration of the order of nanosecond for fully explicit DNS. Availability and accuracy of these numerical methods have been confirmed carefully for auto-ignition, planar laminar flame and turbulent premixed flames. To realize DNS of IC engine with realistic kinetic mechanism, several DNS of elemental combustion process in IC engines has been conducted.

Keywords: Direct Numerical Simulation, Turbulent Combustion, Internal Combustion Engine, Detailed Kinetic Mechanism

1. INTRODUCTION

Turbulent combustion is one of the most difficult problems in computational science, because this phenomenon includes very complicated interaction of turbulence and chemical reaction. In the combustion chemistry, very fast elementary reactions cause quite small time and spatial scales, which is well known as the stiffness problem. Direct numerical simulations (DNS) of turbulent flows have been used for turbulence research in last few decades, whereas the first three-dimensional DNS of turbulent combustion with detailed kinetic mechanism has reported in 2000[1]. In this paper, current state and perspective of DNS of turbulence and turbulent combustion are discussed with feature trend of the fastest supercomputer in the world. Based on the perspective of DNS of turbulent combustion, possibility of perfect simulations of IC engine is shown. Since the recent development of three-dimensional DNS of turbulent combustion is reviewed in[2], several DNS of elemental combustion process in IC engines are presented in this paper.

High efficiency and low emission are of great significance for researches on internal combustion engines. Although emissions of spark ignition engine can be controlled effectively, the fuel economy is poor because of its low compression ratio. In contrast, although diesel engines are attractive because of their high thermal efficiency, nitrogen oxide (NOx) and particulate matter (PM) emissions from them are high and difficult to reduce simultaneously. The thermal NOx and PM generation mechanism indicates that it is better to find a low temperature combustion mode with homogeneous charge for the control of formation of NOx and PM. Therefore, homogeneous charge compression ignition (HCCI) engine is expected as one of the promising combustion technology.

In HCCI engine, the lean premixed fuel-air is automatically ignited by mixture compression. The HCCI engine has potential for higher efficiency compared with spark ignition engine, and lower emission compared with diesel engine. However, there are a lot of issues to realize HCCI engine practically. Narrow operating load range and engine noise are some examples of the problems. The most serious issue is the control of ignition. Many researchers have studied to overcome this issue experimentally (e. g. EGR, fuel reforming, etc.)[3-5], whereas the flame structures in the combustion chamber have not been clarified yet. Combustion modes in HCCI engine can be regarded as turbulent premixed flames because of premixed mixture and inhomogeneous flow field.

In our previous studies[1, 6-7], we have conducted DNS of hydrogen-air turbulent premixed flames in three dimensional homogeneous isotropic turbulence with a detailed kinetic mechanism and have shown that the fine-scale structure in the unburnt side plays quite important roles on the local flame structure. Therefore, it is considered that the characteristics of turbulence are very important for ignition and propagation process of the mixture. To clarify mechanisms of ignition and propagation in turbulence, numerical approach is powerful because it is difficult to measure the local flame structure in turbulence experimentally.

In this paper, DNS of ignition/propagation and auto-ignition of turbulent premixed flames has been conducted to investigate turbulent combustion mechanism in PCCI and HCCI engines. DNS are conducted for hydrogen/air, methane/air and n-heptane/ air mixtures by considering detailed or reduced kinetic mechanism. Effects of turbulence, Reynolds number and pressure on the ignition and propagation process are investigated by DNS of ignition and propagation of hydrogen/air, methane/air and n-heptane/air premixed flame in homogeneous isotropic turbulence. Furthermore, effects of turbulence and initial inhomogeneity of the mixture on auto-ignition process are investigated by DNS of auto-ignition of turbulent homogeneous or inhomogeneous methane/air mixture.

2. HUGE DNS OF TURBULENCE AND TURBULENT COMBUSTION

Figure 1 shows a result of the largest three-dimensional DNS of turbulent premixed flame[8]. In this DNS, a detailed kinetic mechanism is considered and several billion grid points are used. Figure 2 shows a trend of the fastest supercomputer in the world (hereafter, #1 SC)[9]. At June, 2007, the #1 SC has about 280TFlops. The fastest supercomputer in Japan is TSUBAME, which has about 49TFlops, in Tokyo Institute of Technology until April, 2007, whereas that is HA8000 at the University of Tokyo now. Recent improvement rate of #1 SC is 10 times in 3.5 years. If this rate is sustained, 1 EXAFlops supercomputer will be realized in 2020, where EXA means 10^{18}. In Fig.2, developments in total grid points used in DNS of nonreactive

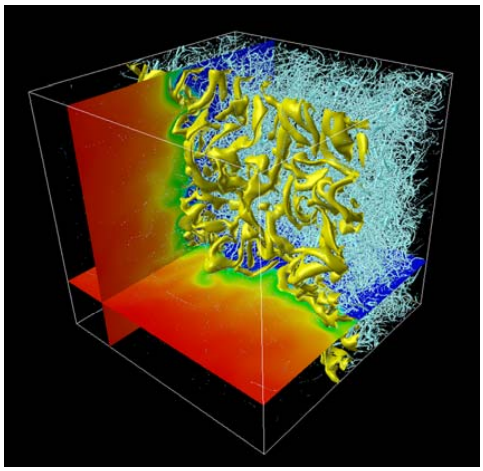

Fig. 1 Largest DNS of turbulent combustion in the world

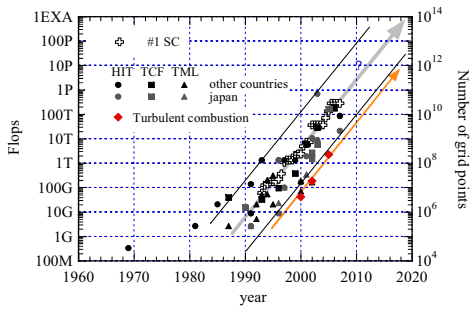

Fig. 2 Development of the fastest supercomputer in the world and grid points of DNS of various turbulence and turbulent combustion.

turbulence are also presented. Here, the plots are split into DNS by Japan and other countries for each fundamental turbulent field (homogeneous isotropic turbulence: HIT, turbulent channel flow: TCF and turbulent mixing layer: TML). The number of grid points used in DNS of turbulence increases with the same rate of the #1 SC. In Japan, new high performance supercomputer is projected and will be constructed in 2011. The promising calculation speed is 10Pflops. Figure 2 suggests that this supercomputer will realize DNS of turbulence with 10^{12} grid points. The trends of the #1 SC and DNS also suggest that DNS with 10^{14} grid points will be reported in 2020.

For numerical simulations of turbulent combustion, one has to solve lots of species conservation equations with mass, momentum and energy conservation equations. The number of species is about 10 for the simplest fuel such as hydrogen and about 50 for methane or propane. For gasoline, several hundreds species should be considered in numerical simulation. The reaction rate of each species is determined from the complicated combinations of elementary reactions. The number of elementary reaction also depends on fuel; about 30 for hydrogen, about 300 for methane or propane and several thousand for gasoline. In general, the flame thickness is less than 1mm. Since temperature, density and species composition changes drastically in very thin flame, transport and thermal properties are also changed. Generally, 10 to 20 grid pints are required to resolve flame. Supposing that Kolmogorov length scale is same with the flame thickness, DNS of turbulent combustion requires about 10^3 times grid points compared with DNS of turbulence for the same Reynolds number. As the number of species (N) also increases for complex fuel, required memory for DNS of turbulent combustion is estimated to of the order of $10^3(N+4)/3$. In addition, since the increment of time integration is limited by the fastest elementary reaction and is of the order of nanosecond, CPU time of DNS of turbulent combustion is about 10^3 times that of incompressible turbulence and about 10 times that of compressible turbulence. Therefore, the first three-dimensional DNS of turbulent combustion with detailed kinetic mechanism has reported in 2000[1].

To show the possibility of the perfect simulation of internal combustion engines, a trend for gird points used in DNS of turbulent combustion is shown in Fig.2. DNS plotted in Fig.2 have been conducted for hydrogen fuel with a detailed kinetic mechanism including 12 reactive species and 27 elementary reactions. From the estimation in above, required memory is about 5×10^3 times that for incompressible turbulence. Figure 2 shows that the number of grid points used in DNS of turbulent combustion is lower than that of turbulence with this factor. The increasing rate of the grid points used in DNS of turbulent combustion also coincides with that of #1 SC similar to DNS of turbulence. If the 10PFlops SC is realized, 10^{10} gird points will be used for DNS of turbulent combustion. For 1EXAFlops, that with 10^{12} will be reported in 2020. Here, it should be noted that this expectation is for hydrogen fuel. In many combustors in engineering applications, hydrocarbon fuels are used. As for the heptane which is one composition of gasoline, a detailed kinetic mechanism will be constructed from 544 reactive species and 2446 elementary reactions. In this case, the number of grid point is reduced to about 30 billion (3100^3). Here, based on the fast three-dimensional DNS of turbulent combustion, CPU time which is required for DNS of a cylinder of an automobile IC engine (1600cc) can be estimated. In Table 1, the estimated CPU time is shown for several calculation speed of computer. Even for the present #1 SC which has 280TFlops, 1000 years are required for the perfect simulation of IC engine. For 10PFlops, 30 years are needed. If the 1EXAFlops SC is realized, this CPU time is reduced to about 4 months. This estimation suggests that DNS of IC engines is possible in 2020.

To shorten CPU time required for DNS of turbulent combustion, two numerical methods are introduced to full-explicit full-compressible DNS code. One is compact finite difference filter to reduce spatial resolution requirements and numerical oscillations in small scales, and another is well-known point-implicit scheme to avoid quite small time integration of the order of nanosecond for fully explicit DNS. Availability and accuracy of these numerical methods have been confirmed carefully for auto-ignition, planar laminar flame and turbulent premixed flames. These modifications reduce the CPU time to 4 days. In addition to these numerical aspects, physical investigations are required for Soret effect, Dufour effect, pressure gradient diffusion, wall-flame interaction, radiation heat transfer, etc.

Table 1 CPU time required for the perfect simulation of IC Engine.

Flops	*CPU hours*	*CPU years*
2G	4.52×10^{11}	5.16×10^{7}
40T	6.78×10^{7}	7.74×10^{3}
100T	2.71×10^{7}	3.10×10^{3}
280T	9.69×10^{6}	1.11×10^{3}
1P	2.71×10^{6}	3.10×10^{2}
10P	2.71×10^{5}	3.10×10^{1}
1EXA	2.71×10^{3}	0.310

Table 2 Numerical parameters of DNS of ignition and propagation of turbulent premixed flames

	ID	P [MPa]	ϕ	Re_λ	u'_{rms}/S_L	l/δ_F	l/δ_L	T_{max} [K]	T_{pre} [K]	r_c [mm]	L [mm]	N
H_2	HR47	0.1	1.0	47.1	0.77	174.3	3.04	1500	800	0.7	10	1025
	HR66	0.1	1.0	66.4	1.93	88.2	1.54	1500	800	0.7	15	1537
	HR71	0.1	1.0	71.9	1.93	78.0	1.36	1500	800	0.7	10	1025
	HR106	0.1	1.0	106.8	1.92	166.7	2.91	1500	800	0.7	10	1025
CH_4	CR47S	0.1	1.0	47.1	3.02	44.4	6.21	2200	950	2.0	10	1025
	CR47W	0.1	1.0	47.1	1.51	88.9	12.43	2200	950	2.0	20	2049
	CR71S	0.1	1.0	71.9	7.54	19.9	2.78	2200	950	2.0	10	1025
	CR71W	0.1	1.0	71.9	3.77	39.7	5.55	2200	950	2.0	20	2049
	CR71WP2	0.2	1.0	71.9	3.86	39.1	5.61	2000	850	1.5	12	2049
	CR71WP5	0.5	1.0	71.9	3.75	40.4	6.14	1900	750	1.0	7	2049
	CR106S	0.1	1.0	106.8	7.50	42.5	5.94	2200	950	2.0	10	1025
	CR106W	0.1	1.0	106.8	3.75	84.9	11.88	2200	950	2.0	20	2049
C_7H_{16}	C7R47	0.1	1.0	47.1	6.42	21.0	2.68	1600	700	1.0	10	513
	C7R106	0.1	1.0	106.8	15.9	20.0	2.74	1600	700	1.0	10	513

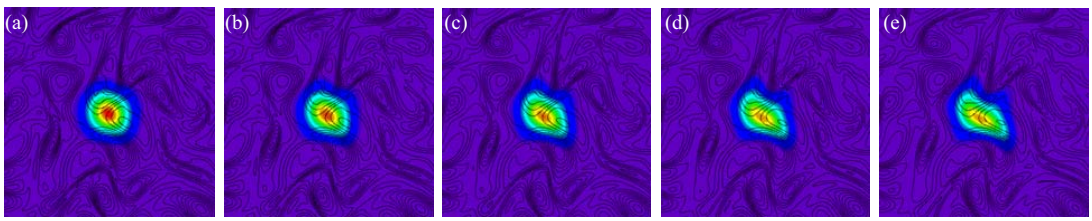

Fig. 2 Temporal developments of temperature and vorticity in induction phase for HR47 ((a) $t/\tau_F = 0.0825$, (b) $t/\tau_F = 0.165$, (c) $t/\tau_F = 0.247$, (d) $t/\tau_F = 0.330$, (e) $t/\tau_F = 0.412$).

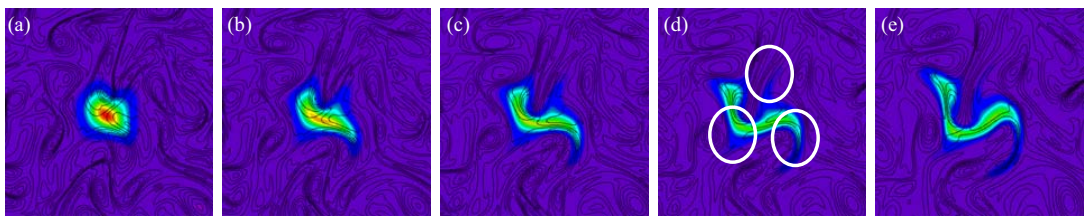

Fig. 3 Temporal developments of temperature and vorticity in induction phase for HR106 ((a) $t/\tau_F = 0.0825$, (b) $t/\tau_F = 0.247$, (c) $t/\tau_F = 0.412$, (d) $t/\tau_F = 0.742$, (e) $t/\tau_F = 0.825$).

3. IGNITION AND PROPAGATION PROCESS OF TURBULENT PREMIXED FLAME

3.1 Direct numerical simulation

In this study, Soret effect, Dufour effect, pressure gradient diffusion, bulk viscosity and radiative heat transfer are assumed to be negligible. From the above assumptions, details of the governing equations have been shown by Miyauchi et al.[10]. A detailed kinetic mechanism which includes 12 reactive species and 27 elementary reactions[11-13] is used for hydrogen/air mixture and GRI Mech. 2.11 (49 reactive species and 279 elementary reactions)[14] is used for methane/air mixture. A reduced kinetic mechanism which includes 38 reactive species and 61 elementary reactions[15] is used for n-heptane/air mixture. The temperature dependence of the viscosity, the thermal conductivity and the diffusion coefficients are considered by linking CHEMKIN packages with modifications for vector/parallel computations.

The governing equations are solved by using a fourth order central finite difference scheme. To damp any spurious high-wave number oscillations, a fourth order compact finite difference filter[16] is used. Navier-Stokes characteristic boundary condition (NSCBC)[17-18] is assumed in all directions. Time integration is implemented by a third order Runge-Kutta scheme. For n-heptane/air cases, reaction source terms in species equations are implemented by implicit method[19].

As an initial condition, high temperature region which is regarded as an ignition kernel is given at the center of computational domain, and the ignition starts from this kernel. Initial temperature distribution (T_{ini}) is given as Gaussian distribution;

$$T_{ini} = (T_{max} - T_{pre}) e^{-\frac{r^2}{2\sigma^2}} + T_{pre}, \quad (1)$$

$$\frac{r_c^2}{2\sigma^2} = ln\left(\frac{T_{max} - T_{pre}}{T_{ig} - T_{pre}}\right), \quad (2)$$

where T_{max} is the maximum temperature of the ignition kernel, T_{pre} is preheat temperature, T_{ig} is auto-ignition temperature, and r_c is radius of the ignition kernel. A premixed mixture is assumed to be uniform for all cases. Numerical parameters of DNS conducted in the present study are listed in Table 2. Here, Re_λ is Reynolds number based on Taylor micro scale. δ_F and δ_L are flame thickness defined by $\delta_F = \nu/S_L$ using kinematic viscosity (ν) in unburned mixture and laminar flame thickness based on temperature gradient, respectively. L and N represent computational domain size and grid points in each direction

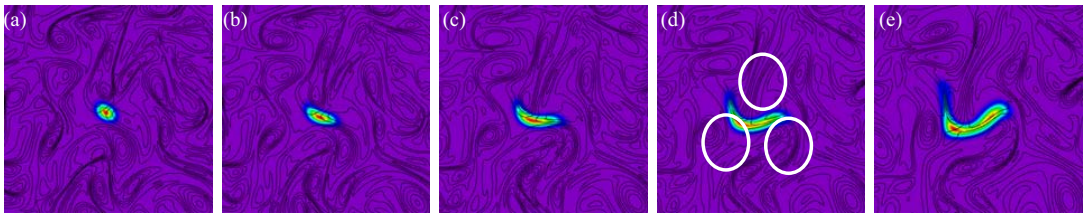

Fig. 5 Temporal developments of mole fraction of H atom with vorticity distribution in induction phase for HR106 ((a) $t/\tau_F = 0.0825$, (b) $t/\tau_F = 0.247$, (c) $t/\tau_F = 0.412$, (d) $t/\tau_F = 0.742$, (e) $t/\tau_F = 0.825$).

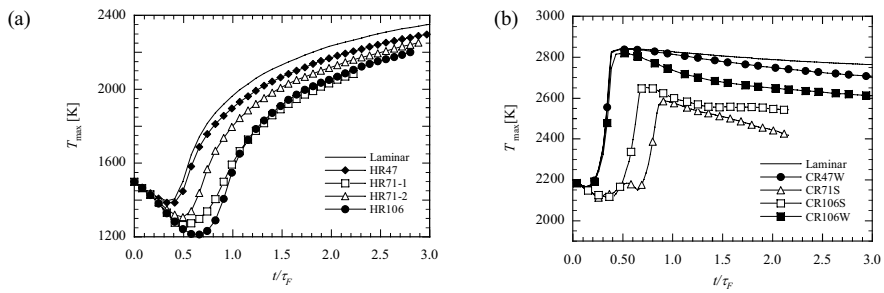

Fig. 6 Temporal developments of maximum temperature for hydrogen/air cases (a) (Laminar, HR47, HR71-1, HR71-2 and HR106) and methane/air cases (b) (Laminar, CR47W, CR71S, CR106S and CR106W).

To investigate the Reynolds number effects on the ignition and propagation process, DNS are conducted with different Reynolds number. In hydrogen/air cases, to clarify the relation between the local structure of turbulence and ignition process, the mixture is ignited from different region in the statistically same turbulent field by adding high temperature region at different point. Effects of ignition point are investigated by setting two patterns in HR47 and five patterns in HR71. The initial turbulent field for these cases is statistically equal to HR106. In methane/air cases, to clarify the effects of pressure, CR71WP2 and CR71WP5 are conducted for high pressure condition.

DNS conditions in the turbulent combustion diagram by Peters[20] are following. CR71W, CR71WP2 and CR71WP5 are located at nearly same position which is near the boundary between corrugated flamelets and thin. reaction zones. HR47 is classified in wrinkled flamelets CR71S, CR106S, C7R47 and C7R106 are classified in thin reaction zones. Other cases are classified in corrugated flamelets. For comparison, laminar conditions are also calculated.

3.2 Effects of turbulence on ignition

Figures 3 and 4 show temporal developments of temperature and vorticity distributions in induction phase before ignition for HR47 and HR106. Here, temperature is denoted by colors and vorticity distribution is shown by contour lines. In HR47 which is low Reynolds number case, high temperature region is slightly stretched by surrounding eddies. In contrast, high temperature region in HR106, which is high Reynolds number and high turbulence intensity case, is distorted tremendously and stretched toward low temperature region by strong eddies.

For the ignition of hydrogen-air mixture, amount of H atom is very important. Figure 5 shows distributions of mole fraction of H atom with vorticity in the induction phase for HR106. The mole fraction is normalized by the maximum value at each time. The distortion of high concentration region of H atom is similar to that of high temperature region. For low Reynolds number case, the distortion of H atom distribution by turbulence is not significant (not shown here). For high turbulence intensity case, however, H atom distribution is strongly distorted by the eddy and H atoms which is transported into low temperature regions disappear as shown by circles in Fig. 5(d). In these regions, productions of intermediate through H atom are suppressed. For hydrocarbon cases, distributions of temperature and intermediate have similar trends.

Figure 6(a) shows temporal developments of the maximum temperature for hydrogen/air cases. Here, HR71-i represents the result from different ignition point in same turbulent flows. The temporal developments of temperature in each case are different. In this study, ignition delay is assumed as period until getting to thermal runaway. Thermal runaway is defined as inflection point of temperature in rapid rise of the maximum temperature. The rise of temperature in HR47 is similar to that of the laminar case, and the difference of ignition delay between HR47 and laminar is small. In contrast, the temperature in HR106 decreases in the induction phase particularly, and the ignition delay is more than twice of the laminar case. The reason is that, as shown in Fig. 4, the degree of distortion of high temperature region is large for HR106, and the high temperature region is distorted such that being separated by the surrounding eddies. This mechanism is interpreted as follows; maintenance of high energy region near the ignition point is difficult due to thermal loss which is caused by distortion (or turbulent diffusion) and cooling of main high temperature region by the eddies, and the resulting suppression of radical production requires much more time for the ignition. The ignition delay tends to increase with turbulence intensity. However, it should be noted that the ignition delay is different even for the same turbulent flow fields if the ignition point was different. As for this difference, discussions will be given later. Figure 6(b) shows temporal developments of the maximum temperature for methane/air cases. For methane/air cases, decrease of the temperature in the induction phase are smaller than that for hydrogen/air cases, and the ignition delay tends to increase with turbulence intensity similar to hydrogen/air cases.

3.3 Effects of turbulence on ignition

Figures 7 and 8 show the temporal developments of distributions of heat release rate and vorticity in propagation

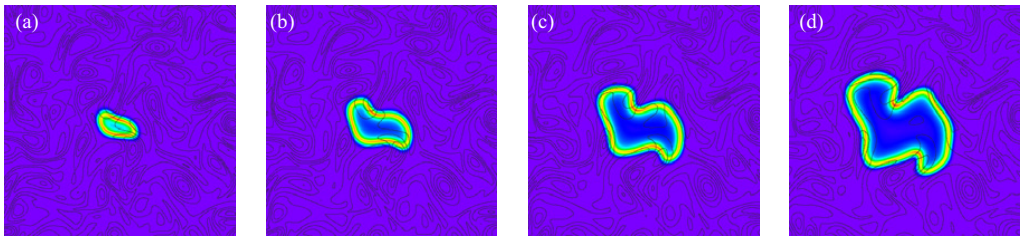

Fig. 7 Temporal developments of distributions of heat release rate and vorticity in propagation process for HR47 ((a) t/τ_F = 0.74, (b) t/τ_F = 1.07, (c) t/τ_F = 1.40, (d) t/τ_F = 1.73).

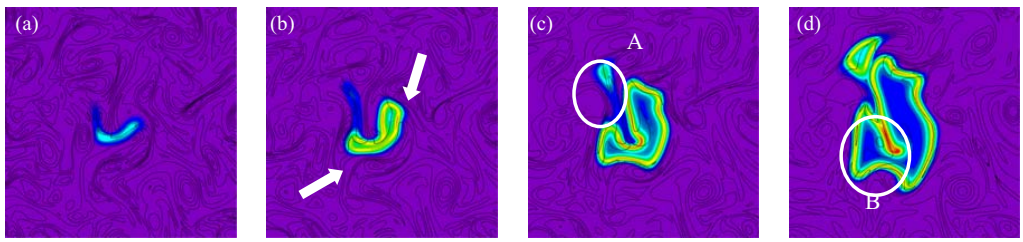

Fig. 8 Temporal developments of distributions of heat release rate and vorticity in propagation process for HR106 ((a) t/τ_F = 0.74, (b) t/τ_F = 1.07, (c) t/τ_F = 1.40, (d) t/τ_F = 1.73).

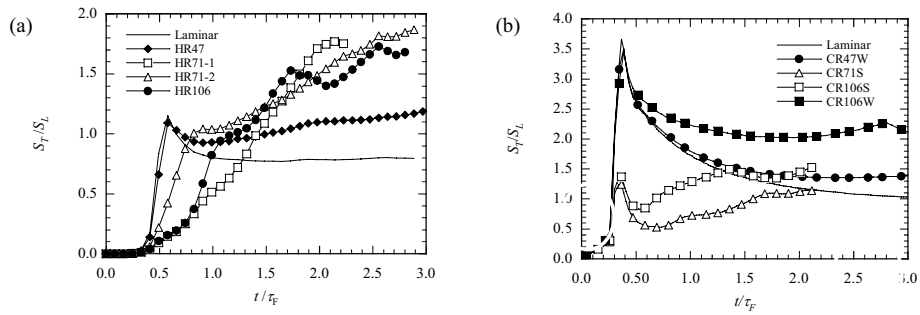

Fig. 9 Temporal developments of the turbulent burning velocity for hydrogen/air cases (Laminar, HR47, HR71-1, HR71-2 and HR106) and methane/air cases (Laminar, CR47W, CR71S, CR106S and CR106W).

process for HR47 and HR106. The heat release rate is normalized by the maximum heat release rate (ΔH_L) of freely propagating laminar flame which includes no effect of flame geometry such as curvature and is approximated as one dimensional. The flame front is stretched and is disturbed its evolution by the strong eddies for both cases. The flame propagates along the edge of eddies as shown by allows in Fig. 8(b). As shown by the circle A, the high temperature region which is separated from the initial ignition kernel in the induction phase is ignited later than main kernel. This result suggests that multiple points ignition with timing difference may occur even for an initial ignition kernel in turbulence. Furthermore, as shown by the circle B, the high heat release rate finally reaches over $1.2\Delta H_L$ at the flame fronts that are enclosed by the burnt gas or that are convex toward the burnt side. The high heat release rate of these flame fronts has also been reported by previous studies on statistically-planer turbulent fronts has also been reported by previous studies on statistically-planer turbulent premixed flame propagating in homogeneous turbulence[1].

These characteristics of the flame structure are reflected in turbulent burning velocity. Figure 9(a) shows the temporal developments of turbulent burning velocity for hydrogen/air cases. The turbulent burning velocity (S_T) is normalized by the laminar burning velocity (S_L) of one-dimensional planer flame. The turbulent burning velocity is defined as follow;

$$S_T = -\frac{1}{\rho_u Y_{H_2,u} l_F} \iint w_{H_2} dxdy, \qquad (3)$$

where ρ_u, $Y_{H2,u}$, l_F and w_{H2} are mixture density, mass fraction of H_2, laminar flame length and reaction rate of H_2, respectively. The subscript u denotes a value in the unburned side. In HR47, the turbulent burning velocity is slightly lower than that of columnar laminar flame until ST reaches SL. Then, ST is always higher than the laminar case. In contrast, it is apparent that the temporal developments of turbulent burning velocity for other cases show different trends compared with the laminar case. It takes a long time until ST reaches SL, which corresponds to the ignition delay shown in Fig. 6(a). In addition, the burning velocity in HR106 shows the rapid rise at about t/τ_F = 1.7, which is caused by appearance of flame elements with high heat release rate as mentioned previously (circle B in Fig. 8 (d)).

Figure 9(b) shows the temporal developments of turbulent burning velocity for methane/air cases. The burning velocity is computed based on consumption rate of CH_4 using a similar definition to Eq. (3). The burning velocity for laminar case, CR47W and CR106W shows the significantly rapid rise just after the ignition, and reaches over three times larger than S_L. Afterwards, S_T decreases in some degree and then it is always higher than the laminar case, as is in the hydrogen cases. Figure 11 shows distributions of heat release rate and

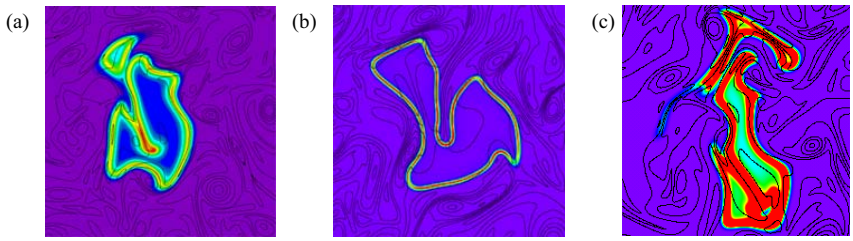

Fig. 10 Distributions of heat release rate and vorticity in propagation process for HR106 (a), CR106W (b) and C7R106 (c) ((a) t/τ_F = 1.73, (b) t/τ_F = 1.95, (c) t/τ_F = 1.85).

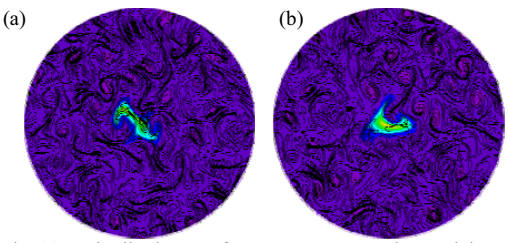

Fig. 12 Distributions of temperature and vorticity in induction phase for HR71-1 (a) and HR71-2 (b) (t/τ_F = 0.412).

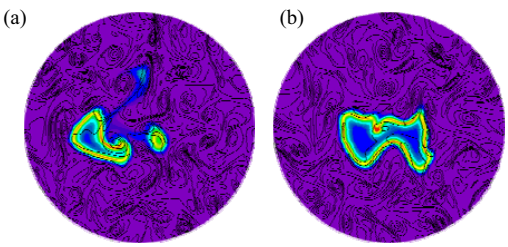

Fig. 13 Distributions of heat release rate and vorticity in propagation process for HR71-1 (a) and HR71-2 (b) (t/τ_F = 1.40).

vorticity in the flame propagation process for different fuel cases. The heat release rate is normalized by corresponding ΔH_L. For hydrocarbon cases, the heat release rates show the significantly rapid rise just after the ignition and high in the whole flame elements compared to that of hydrogen case.

3.3 Effects of local turbulence characteristics

Figure 12 shows distributions of temperature and vorticity in the induction phase for HR71 with different ignition point. In each case, the ignition kernel is given at different points in the statistically same turbulent field. The high temperature region is stretched by eddies in a different way for each case. As shown in Fig. 6(a), the temporal developments of the maximum temperature show that the ignition delay is different even if the turbulent field is statistically same. Therefore, it is considered that the ignition delay significantly depends on local characteristics of turbulence. Figure 13 shows distributions of heat release rate and vorticity in the propagation process for HR71. In HR71-1, the ignition takes place from three points with different timing, while the ignition in HR71-2 takes place only from one point. In addition, it is apparent that the temporal developments of the turbulent burning velocity of these cases are different as shown in Fig. 9(a).

These results imply that consideration of local ignition delay. Figure 14 shows relation between the ignition delay (t') and mean strain rate ($<S_{ij}S_{ij}>$) for characteristics of turbulence

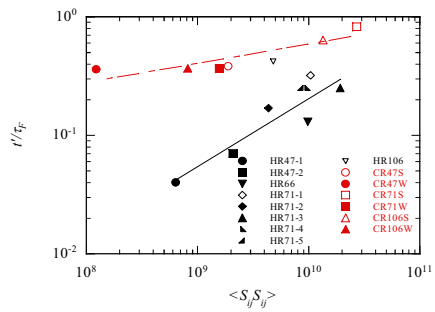

Fig. 14 Relation between ignition delay and mean strain rate.

is important for estimation of the hydrogen/air and methane/air cases. Mean strain rate represents an average of strain rate which is in the region of initial ignition kernel. The ignition delay tends to increase with increase of mean strain rate except for HR71-1 and HR106. In HR71-1 and HR106, the flames are ignited from several points since the initial high temperature region is separated by eddies (Figs. 7 and 12(a)), and the ignition delay additionally increases compared to other cases. Increasing rate of the ignition delay for hydrogen/air cases is larger than that for methane/air cases. This might be caused by the reason that total energy given at initial high temperature region is different. Since initial energy for methane/air cases is larger than that for hydrogen/air cases, the radical production required for ignition is enhanced and the ignition occurs earlier. This leads to decrease of total thermal loss caused by turbulent diffusion in the induction phase.

4. AUTO-IGNITION OF TURBULENT PRE-MIXED FLAME

4.1 Direct Numerical Simulation

Numerical methods used in DNS of auto-ignition of turbulent premixed flames are similar to those in DNS of ignition and propagation in previous sections except for the boundary conditions and initial conditions. The boundary conditions are changed to periodic boundary conditions in all directions to investigate the auto-ignition in a constant volume. Initial temperature of the unburnt mixture is set to higher than auto-ignition temperature without an ignition kernel and two-dimensional homogeneous isotropic turbulence is used for the initial velocity field. DNS are conducted for two different initial temperature (T_{ini} =1750K and 2000K), two different Reynolds number (Re_λ=47 and 106) and two different pressure (P_{ini}=0.1MPa and 0.2MPa). In Table 3, ϕ' denotes fluctuation in equivalence ratio of the initial mixture. The initial fluctuation of the equivalence ratio is given randomly in space independent to the initial turbulent field. The integral length

Table 3 Numerical conditions of DNS of auto-ignition of turbulent premixed flames

ID	T_{ini}[K]	Re_λ	P_{ini}[MPa]	ϕ	ϕ'	*L*[mm]	*N*
CR47F10-00T1P1	1750	47	0.1	1.0	0.0	10	512
CR106F10-00T1P1	1750	106	0.1	1.0	0.0	10	512
CR106F10-00T2P1	2000	106	0.1	1.0	0.0	10	512
CR106F10-00T1P2	1750	106	0.2	1.0	0.0	10	512
CR106F10-00T2P2	2000	106	0.2	1.0	0.0	10	512
CR47F10-01T1P2	1750	47	0.2	1.0	0.1	10	512
CR106F10-01T1P1	1750	106	0.1	1.0	0.1	10	512
CR106F10-01T2P1	2000	106	0.1	1.0	0.1	10	512
CR106F10-01T1P2	1750	106	0.2	1.0	0.1	10	512
CR106F10-02T1P2	1750	106	0.2	1.0	0.2	10	512

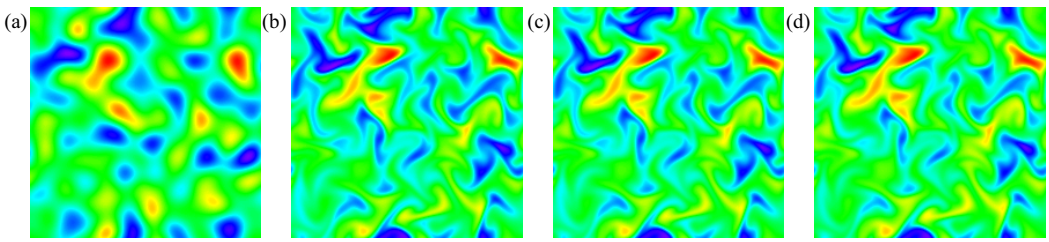

Fig. 15 Development of mole fraction of CH_4 in the auto-ignition process of inhomogeneous mixture (ϕ'=0.2) for Re_λ=106, T_{ini}=1750K and P_{ini}=0.2 MPa. (a): t = 0, mole fraction range[0.079, 0.11], (b): t=82μs, mole fraction range[0.049, 0.082], (c): t=84μs, mole fraction range[0.04, 0.077], and (d): t=86μs, mole fraction range[0.026, 0.07].

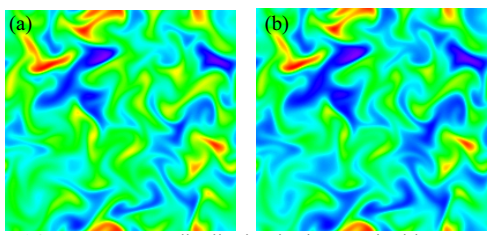

Fig. 16 Temperature distribution in the auto-ignition process of inhomogeneous mixture (ϕ'=0.2) for Re_λ=106, T_{ini}=1750K and P_{ini}=0.2 MPa. (a): t=82μs, temperature range[1879.44, 1941.26(K)] and (b): t=86μs, temperature range[1970.46, 2158.99(K)].

scale of the initial mixture fluctuation is of the order of that of turbulence. To investigate pure turbulence effects on the auto-ignition process, five DNS are conducted for homogeneous mixture. Other five DNS are conducted for inhomogeneous conditions to investigate the effects of non-perfect mixing of the fuel and air on the auto-ignition process. In addition to DNS listed in Table 3, DNS for hydrogen/air mixture is conducted. However, since effects of initial turbulence and inhomogeneity of the initial mixture scarcely affect the global phenomena due to short ignition time and large diffusivity of hydrogen, the results for hydrogen/air mixture are not shown here. Furthermore, zero-dimensional analyses are also conducted for same temperature and equivalence ratio for comparison.

4.2 Effects of turbulence

To investigate effects of turbulent energy dissipation rate (or temperature fluctuation due to turbulence) on the auto-ignition process, DNS for turbulent homogeneous mixture were conducted. Temperature tends to decrease near the center of large vortical structure and to increase in high strain rate regions. Intensity of the temperature fluctuation is higher for high initial temperature and for high initial pressure. However, this fluctuation is significantly low and scarcely affects the global nature of the auto-ignition. Temperature trend does not show any modifications by turbulence. It should be noted that these results were obtained from two-dimensional turbulence. Real three-dimensional turbulence will produce higher temperature fluctuation due to the strong dissipative structure. Therefore, the auto-ignition process might by affected by turbulence even for homogeneous mixture. This issue will be investigated in future works.

4.3 Effects of inhomogeneity

Effects of turbulence and inhomogeneity of the initial mixture are investigated by superposing fluctuation of equivalence ratio. In Fig. 15, development of CH_4 mole fraction in the auto-ignition process of inhomogeneous mixture (ϕ'=0.2) is shown for Re_λ=106, T_{ini}=1750K and P_{ini}=0.2 MPa. As shown in Fig. 15 (a), characteristic length scale of inhomogeneity of the mixture is set to relatively large and is of the order of integral length scale of turbulence. Since the auto-ignition process proceeds in a short time, global mole fraction pattern is approximately similar through the ignition. The regions with low equivalence ratio consume fuel earlier and those with high equivalence ratio do slowly. With the time, difference of fuel concentration in both regions increases. Figure 16 shows typical temperature distribution in the auto-ignition process of inhomogeneous mixture. As the ignition takes place in the regions with low equivalence ratio earlier, temperature in those regions also increases. Temperature difference between low and high equivalence ratio regions is intensified with time. For the case of ϕ'=0.2, Re_λ=106, T_{ini}=1750K and P_{ini}=0.2 MPa shown in Figs. 15 and 16, temperature difference about 200 K is observed at t=86μs.

Temperature trends of the mixture ϕ'=0.1 are shown in Fig. 17 for different Reynolds number cases. For comparison, zero-dimension analysis results for ϕ=0.9, 1.0 and 1.1 are also plotted. The turbulent and inhomogeneous cases ignite at same time with corresponding laminar case approximately. Although temperature fluctuation is relatively high as shown in Fig. 16, the maximum and minimum temperature in Fig. 20

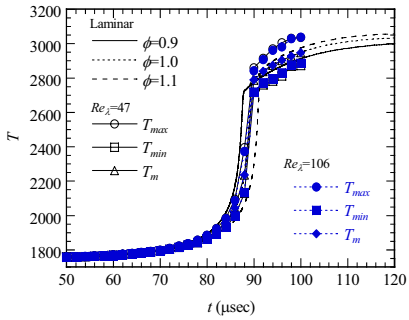

Fig. 17 Effects of Reynolds number on temperature developments for inhomogeneous mixture (ϕ'=0.1) for T_{ini}=1750K and P_{ini}=0.2 MPa.

increase drastically at the same instance. For laminar and homogeneous cases, the initial delay is shorter for lower equivalence ratio. If the auto-ignition process of the inhomogeneous mixture was dominated by local phenomena which is determined by local equivalence ratio, it might be expected that maximum and minimum temperature trends in Fig. 17 coincide with that of corresponding equivalence ratio. However, the obtained results are far from this expectation. Therefore, heat flux from high temperature (or low equivalence ratio) region to low temperature (or high equivalence ratio) region or mass flux from high equivalence ratio region to low equivalence ratio might be important for the global ignition characteristics. This result suggests that the global auto-ignition process of inhomogeneous mixture is controlled by mean equivalence ratio in the initial mixture. The difference between maximum and minimum temperature is larger for low Reynolds number case. Since turbulent diffusion or turbulent mixing works for reduction of inhomogeneity of the mixture, temperature fluctuation is decreased for high Reynolds number case.

5. SUMMARY

In this paper, current state and perspective of DNS of turbulence and turbulent combustion are discussed with feature trend of the fastest supercomputer in the world. Based on the perspective of DNS of turbulent combustion, possibility of perfect simulations of IC engine is shown. In addition, DNS of ignition/propagation and auto-ignition of turbulent premixed flames are presented as examples for investigation of turbulent combustion mechanism in PCCI and HCCI engines.

ACKNOWLEDGMENTS]

This work is partially supported by Grant-in-Aid for Scientific Research (B) (No.19360097) and Grant-in-Aid for Young Scientists (S) (No. 20676004) of Japan Society for the Promotion of Science.

REFERENCES

[1] 2000, Tanahashi, M., Fujimura M. and Miyauchi, T., "Coherent fine scale eddies in turbulent premixed flames," *Proc. Combust. Inst*., Vol.28, pp.529-535.

[2] 2008, Tanahashi, M., Sato, M., Shimura, M. and Miyauchi, T., "DNS and laser diagnostics of turbulent premixed flames," *J. Thermal Sci. and Tech*., Vol.3, No.3, pp.391-409.

[3] 1999, Kaimai, T., Tsunemoto, H. and Ishitani, H., "Effects of a Hybrid Fuel System with Diesel and Premixed DME/Methane Charge on Exhaust Emissions in a Small DI Diesel Engine," *SAE Technical Paper*, 1999-01-1509, 1-7.

[4] 2001, Stanglmaier, R.H., Ryan III, T.W. and Souder, J. S., "HCCI Operation of a Dual-Fuel Natural Gas Engine for Improved Fuel Efficiency and Ultra-Low NOx Emission at Low to Moderate Engine Loads," *SAE Technical Paper*, 2001-01-1897, 1-7.

[5] 2002, Law, D., Allen, J. and Chen, R., "On the Mechanism of Controlled Auto Ignition," *SAE Technical Paper*, 2002-01-0421, 1-9.

[6] 2002, Tanahashi, M., Nada, Y., Ito Y. and Miyauchi, T., "Local flame structure in the well-stirred reactor regime," *Proc. Combust. Inst*., Vol.29, pp.2041-2049.

[7] 2004, Nada, Y., Tanahashi, M. and Miyauchi, T., "Effect of turbulence characteristics on local flame structure of H2-air premixed flames," *J. Turbulence*, 5 , pn. 16.

[8] 2007, Tanahashi, M., Nada, Y., Shiwaku, N. and Miyauchi, T., "Direct Numerical Simulations of Turbulent Premixed Flames with Realistic Kinetic Mechanisms," *Frontiers of Computational Science*, Eds. Y. Kaneda, H. Kawamura, M. Sasai, Springer, pp.107-113.

[9] http://www.top500.org/

[10] 1996, Miyauchi, T., Tanahashi, M., Sasaki, K. and Ozeki, T., "Vortex-Flame Interaction in Diffusion Flames," *Transport Phenomena in Combustion*. Chen, C. H. ed., Taylor and Francis, New York, pp.1095-1105.

[11] 1989, Miller, J.A. and Bowman, C.T., "Mechanism and Modeling of Nitrogen Chemistry in Combustion," *Prog. Energy Combust. Sci*., Vol.15, pp.287-338.

[12] 1991, Smooke, M.D. and Giovangigli, V., "Formulation of the Premixed and Nonpremixed Test Problems," *Reduced Kinetic Mechanisms and Asymptotic Approximations for Methane-Air Flames*, Springer-Verlag, pp.1-28.

[13] 1986, Kee, R.J., Dixon-Lewis, G., Warnatz, J., Coltrin, M.E. and Miller, J.A., "A Fortran Computer Code Package for the Evaluation of Gas-Phase Multicomponent Transport Properties," *Sandia Report*, SAND86-8246.

[14] Bowman C.T., Hanson R.K., Davidson D.F., Gardliner Jr. W.C., Lissianski V., Smith G.P., Golden D.M., Frenklach M. and Goldenberg M., Available from: http://www.me.berkeley.edu/gri_mech.

[15] 2006, Maroteaux, F. and Noel, L., "Development of a Reduced N-heptane Oxidation Mechanism for HCCI Combustion Modeling," *Combust. Flame*, Vol.146, pp.246-267.

[16] 1992, Lele, S.K., "Compact Finite Difference Schemes with Spectral-like Resolution," *J. Comput. Phys.*, Vol.103, pp.16-42.

[17] 1992, Poinsot, T.J. and Lele, S.K., "Boundary Conditions for Direct Simulations of Compressible Viscous Flows," *J. Comput. Phys*., Vol.101, pp.104-129.

[18] 1994, Baum, M., Poinsot, T. and Thevenin, D., "Accurate Boundary Conditions for Multicomponent Reactive Flows," *J. Comput. Phys*., Vol.116, pp.247-261.

[19] 1989, Brown, P. N., Byrne, G. D. and Hindmarsh, A. C., "VODE, A Variable-coefficient ODE Solver," *SIAM J. Sci. Stat. Comput*., Vol.10, pp.1038-1051.

[20] 1999, Peters, N., "The Turbulent Burning Velocity for Large-Scale and Small-Scale Turbulence," *J. Fluid Mech*., Vol.384, pp.107-132.